Enhancement of the recoil effect in x-ray photoelectron spectra of molecules driven by a strong ir field

V. C. Felicíssimo,[1,2] F. F. Guimarães,[1,2] and F. Gel'mukhanov[1,*]

[1]*Theoretical Chemistry, Roslagstullsbacken 15, Royal Institute of Technology, S-106 91 Stockholm, Sweden*
[2]*Departamento de Química, Universidade Federal de Minas Gerais, Av. Antonio Carlos, 6627, CEP-31270-901,*
Belo Horizonte, MG, Brazil
(Received 17 March 2005; published 19 August 2005)

The C K and O K x-ray photoelectron spectra of the CO molecule, driven by a strong ir field, are studied theoretically. An enhancement of the recoil effect, which results in a strong dependence of the electron vibrational profile on the energy of x-ray photon, is found. The enhancement of the recoil effect happens due to an ir-induced increase of the wave-packet size. An extra enhancement occurs when the gradients of ground and ionized states approach each other. Under an increase of the photon energy, different sides of the x-ray photoelectron band experience blue- and redshifts, which are related to the difference of the gradients of the ground and core ionized states in the points of the vertical transitions near turning points of the wave packet. This makes the ir–x-ray pump-probe spectroscopy a very promising tool to study the shape of the potential energy surfaces.

I. INTRODUCTION

The x-ray photoelectron spectroscopy [(XPS), or ESCA (electron spectroscopy for chemical analysis)] is the most reliable method known for quantitative studies of the composition and chemical environment of molecular systems [1]. Ionization of a core electron is generally accompanied by vibrational excitations due to changes in the molecular potential. The vibrational structure of XPS spectra gives additional information about the molecular structure and interaction of the molecule with the environment. One of the interesting aspects of this phenomenon is the photon energy dependence, which is quite strong near the shape resonances, where the energy of the photoelectron is rather small [2,3]. For higher energies, when the wavelength of the photoelectron becomes comparable to the size of the vibrational wave function, the momentum of the photoelectron starts to influence the Franck-Condon (FC) distribution [4,5]. This effect is pronounced at rather high energies of the photoelectron (>2 keV) in standard XPS measurements with molecules in the lowest vibrational state [5].

Recent developments in the generation and utilization of brilliant x-ray and ultrashort infrared (ir) pulses open opportunities for XPS studies of molecules driven by a strong ir field [6]. The strong ir and mid-ir pulses [7–10] excite molecules in high vibrational states. One can expect that the photoelectron momentum starts to be important for lower x-ray photon energies because of the larger size of the ir-induced vibrational wave packet.

The aim of this paper is to study the x-ray photoelectron spectra of molecular systems driven by a strong ir field. The main effect, discussed here, is the role of the photoelectron on the vibrational structure of XPS spectra of molecules driven by strong ir radiation. We show that an ir field enhances the manifestation of the recoil effect through the formation of an extensive vibrational wave packet in the ground electronic state. The momentum of the photoelectron makes the x-ray transition nonvertical. This leads to a shift of the sidebands related to the classical turning points, as well as to the splitting of the XPS profile, which grows with an increase of the x-ray photon energy. The manifestation of the recoil effect is very sensitive to the shape of the interatomic potentials, namely, to the ratio of the gradients of the ground-state and core-ionized-state potentials in the classical turning points of the nuclear wave packet. The enhancement of the recoil effect happens because of an ir-induced increase of the wave-packet size. An extra enhancement occurs when the gradients of the ground and ionized states approach each other. It is worth noting that rather long x-ray pulses can be used in studies of the discussed recoil effect. The only restriction is that the pulse duration has to be shorter than the lifetime of vibrational level in the ground electronic state (~1 ns to 1 ps).

This paper is organized as follows. We start in Sec. II by describing the physical picture of the recoil effect enhancement in the field of a strong ir laser. The computational details are elucidated in Sec. III. We analyze the x-ray photoelectron spectra of molecules driven by a strong ir field in Sec. IV. Our findings are summarized in Sec. V.

II. PHYSICAL PICTURE OF THE PHASE SENSITIVITY OF X-RAY ABSORPTION SPECTRUM

We consider molecules that interact with the ir pump field L and high-frequency probe x-ray radiation X (see Fig. 1)

$$\mathcal{E}_\alpha(t) = \mathbf{E}_\alpha(t)\cos(\omega_\alpha t - \mathbf{k}_\alpha \cdot \mathbf{R} + \varphi_\alpha), \quad \alpha = L,X. \quad (1)$$

Atomic units are used throughout the whole section. The pump and probe fields, $\mathbf{E}_\alpha(t) = \mathbf{e}_\alpha E_\alpha(t)$, are characterized by

---

*Permanent address: Institute of Automation and Electrometry, 630090 Novosibirsk, Russia

023414-1
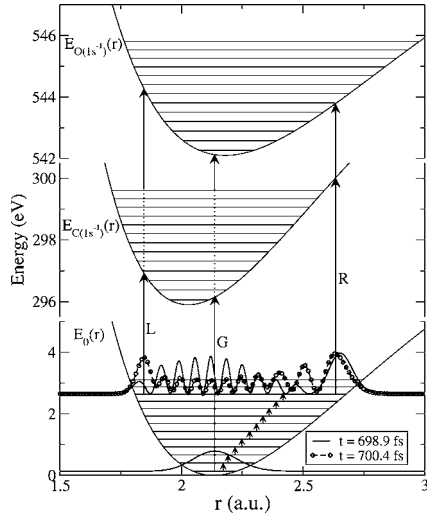
FIG. 1. Scheme of ir–x-ray pump probe transitions. The wave packet, $|\phi|$, induced by the ir field is depicted by broken line with circles for $t=700.4$ and solid line for $t=698.9$ fs. The "ladder" of ir transitions is depicted by short vertical arrows, whereas long vertical arrows show the x-ray transitions. The left and the right classical turning points of the ir-induced wave packets are $r_L=1.846$ a.u. and $r_R=2.632$ a.u., respectively.

the polarization $\mathbf{e}_\alpha$ and wave $\mathbf{k}_\alpha$ vectors, envelopes $E_\alpha(t)$, frequencies ω_α, and phases φ_α.

To be specific, we consider x-ray photoionization of the $1s$ orbital of the atom A in the diatomic molecule AB. Because of the locality of the x-ray transition, the wave functions of the x-ray photon and outgoing photoelectron imply a phase factor in the electronic transition matrix element

$$e^{-\iota \mathbf{q} \cdot \mathbf{R}_A}, \quad \mathbf{q} = \mathbf{p} - \mathbf{k}_X, \tag{2}$$

which depends on the photon momentum $\mathbf{k}_X$, on the photoelectron momentum $\mathbf{p}$, and on the coordinate of the core ionized atom A, $\mathbf{R}_A = \mathbf{R}_c + \alpha \mathbf{r}$. Here, $\mathbf{R}_c$ is the coordinate of the center of mass, $\mathbf{r} = \mathbf{R}_A - \mathbf{R}_B$ is the internuclear separation, $\alpha = m_B/(m_A + m_B)$, where m_A and m_B are masses of atoms A and B, respectively.

The phase factor (2) modifies the generalized Franck-Condon amplitude

$$\langle \nu | \nu_0 \rangle \langle \pi | \pi_0 \rangle \rightarrow f = \langle \nu | e^{-\iota \alpha \mathbf{q} \cdot \mathbf{r}} | \nu_0 \rangle \langle \pi | e^{-\iota \mathbf{q} \cdot \mathbf{R}_c} | \pi_0 \rangle$$
$$= \langle \nu | e^{-\iota \alpha \mathbf{q} \cdot \mathbf{r}} | \nu_0 \rangle \delta(\pi - \pi_0 + \mathbf{q}) \tag{3}$$

Here, $|\nu\rangle$ is the νth vibrational state, while $|\pi\rangle = (2\pi)^{-3/2} \exp(\iota \pi \cdot \mathbf{R}_c)$ is the wave function of the molecular center of gravity with momentum π. The FC amplitude $\langle \pi | \exp(-\iota \mathbf{q} \cdot \mathbf{R}_c) | \pi_0 \rangle$ results in the momentum conservation law $\pi = \pi_0 - \mathbf{q}$. This and Eq. (3) allows one to conclude that the internal molecular motion gets the recoil momentum $-\alpha \mathbf{q}$. The vibrations occur along the molecular axis, and because of this, the vibrational degrees of freedom get the momentum
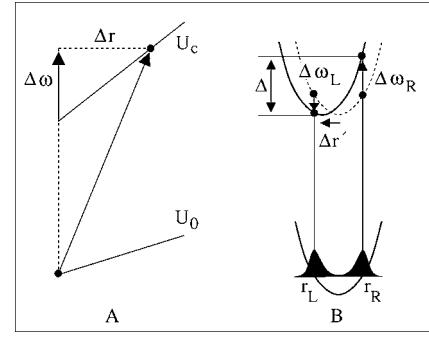
FIG. 2. Physical picture of Eqs. (7) and (16). (a) Different potentials of the ground and core ionized states, $F_c \neq F_0$. (b) The same potentials of the ground and core ionized states.

$$- \alpha q \cos \theta, \tag{4}$$

where θ is the angle between $\mathbf{q}$ and the molecular axis. The atom A changes its momentum due to the absorption of the x-ray photon and the ejection of the photoelectron. This momentum is transfered to the center of gravity, $\pi = \pi_0 - \mathbf{q}$, as well as to the internal degrees of freedom (4). The center of gravity and internal degrees of freedom of the molecule get the recoil energies

$$E_{\text{rec}} = \frac{q^2}{2M}, \quad E_{\text{rec}}^{(i)} = E_{\text{rec}} \frac{m_B}{m_A} \cos^2 \theta = \frac{(\alpha q \cos^2 \theta)^2}{2\mu}, \tag{5}$$

respectively. Here, $M = m_A + m_B$ and $\mu = m_a m_B / M$.

A. Shifts of the sidebands

As one can see from Fig. 1, the strong ir field creates a wave packet that has maxima near left (L) and right (R) classical turning points ($r = r_L$ and $r = r_R$), where the kinetic energy is equal to zero. The x-ray transitions from these points result in two bands in the XPS spectrum. Let us consider the case when the gradients of the ground (F_0) and of the core ionized (F_c) potentials are different in the point of vertical transition $F_0 \neq F_c$. The situation with equal potentials for both the ground and core ionized states is considered in Sec. IV D. The internal recoil energy $E_{\text{rec}}^{(i)}$ (5) increases the kinetic energy of the molecule in the core ionized state. However, the probability of core ionization takes maximum near the classical turning point where this kinetic energy is equal to zero. This happens only if the transition is not vertical, and it takes place in a point shifted by [see also Fig. 2(a)],

$$\Delta r = \frac{E_{\text{rec}}^{(i)}}{F_c - F_0}. \tag{6}$$

In this point, the recoil energy $E_{\text{rec}}^{(i)}$ is compensated by the change of the potential energy $(F_c - F_0) \Delta r$. Here, $F_i = dU_i/dr$ is the gradient in the point of vertical transition $r = r_L$ or $r = r_R$ (Fig. 1). As one can see from Fig. 2(a), this leads to a shift of the XPS band
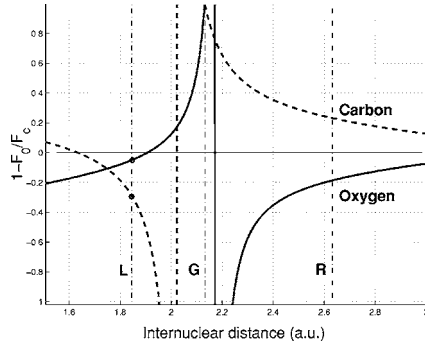
FIG. 3. Relative difference between the gradients of the core-ionized- and ground-state potentials vs the internuclear distance r of the CO molecule. Solid and dashed lines show $1-F_c/F_0$ for $O(1s^{-1})$ and $C(1s^{-1})$ core ionized states, respectively. Vertical dashed-dotted lines mark the positions of the right (R) and of the left (L) turning points, as well as, the equilibrium distance of the ground state (G).

$$\Delta\omega = F_c\Delta r = \frac{E_{rec}^{(i)}}{1-F_0/F_c} \approx (\omega_X - I_{1s})\frac{(m_B/m_A)\cos^2\theta}{M(1-F_0/F_c)}. \quad (7)$$

The strict derivation of this equation is given in the Appendix. We neglect the momentum of the x-ray photon at the right-hand side of Eq. (7), which is small in the studied energy region. It is worth emphasizing that the shift (7) increases when the ratio of the gradients F_0/F_c approaches unity (see Fig. 3).

Apparently, the peak position of individual vibrational peaks does not experience the shift given by Eq. (7). Only the centers of gravity of the L or R sidebands are shifted. This effect is discussed in detail in Sec. IV B.

III. COMPUTATIONAL DETAILS

The propagations of the vibrational wave packets are calculated using Morse potentials $E(r)=D\{1-\exp[-\zeta(r-r_e)]\}^2$ for ground and core ionized states with the parameters from Refs. [11–13] (see Table I), where $D=\omega_e^2/(4\omega_e x_e)$, $\zeta = \sqrt{2\mu\omega_e x_e}$. The vibrational frequency of the CO ground state is 0.266 eV, while the core ionized states of carbon and oxygen have vibrational frequencies 0.322 and 0.240 eV, respectively. The shapes of the ir and x-ray pulses are modeled by

TABLE I. Spectroscopic constants of CO used in the simulations: vibrational frequencies, anharmonicity constants, internuclear distances and ionization potentials.

Spectr. const.	CO $(X^1\Sigma^+)^a$	C $(1s^{-1})$ $(^2\Sigma^+)^b$	O $(1s^{-1})$ $(^2\Sigma^+)^c$
ω_e (cm^{-1})	2169.813	2599	1931.7
$\omega_e x_e$ (cm^{-1})	13.2883	15.92	10.93
r_e (Å)	1.128323	1.073	1.153
I_{1s} (eV)	0	295.9	542.1

[a]Reference 11.
[b]Reference 12.
[c]Reference 13.
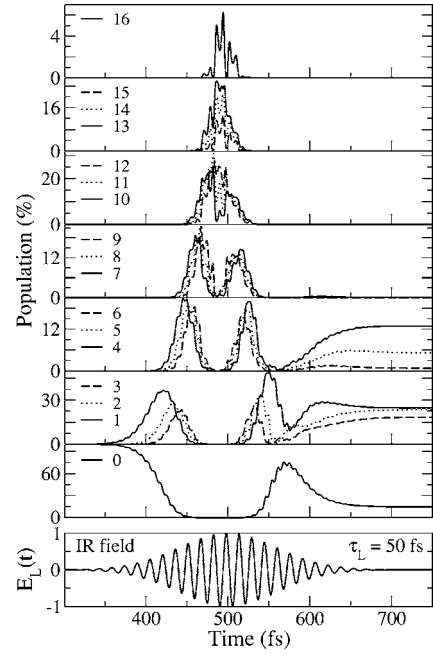
FIG. 4. Dynamics of populations ρ_ν of ground state vibrational levels $\nu=0,\ldots,16$ for $I_L=2.3\times10^{14}$ W/cm^2, $t_L=500$ fs, and a long ir pulse $\tau=50$ fs. The lowest panel displays the amplitude of the ir field normalized to the maximum.

Gaussian functions: $I_i\exp\{-[(t-t_i)/\tau_i]^2\ln 2\}$, $i=L,X$. $I_L=2.3\times10^{14}$ W/cm^2; $t_L=200$ fs, $\tau_L=25$ fs (everywhere except in Fig. 4); $\tau_X=3$ and 10 fs; the delay time $\Delta t=t_X-t_L=500$ fs. $\omega_L=\omega_{10}=0.266$ eV and $\varphi_L=0.9215$ rad. The r dependence of the permanent dipole moment $\mathbf{d}(r)$ in the ground state is computed by the CASSCF method using the DALTON program [14] and aug-cc-pVDZ basis set [15,16]. A complete active space (CAS) formed by 10 electrons in 10 orbitals (carbon and oxygen L shells) is employed. The C K and O K electrons are kept inactive. The momentum of the photon is small in the studied energy region and is neglected in the simulations. Because of this, θ is now the angle between $\mathbf{p}$ and the molecular axis and $q\approx p$. All simulations are performed for oriented molecules: $\theta=0$ deg and $\theta=90$ deg. The role of the recoil effect is the biggest one for $\theta=0$ deg, whereas it does not influence the XPS spectrum when $\theta=90$ deg.

The calculations of the XPS spectra of CO molecule driven by an ir field are based on the theory developed in our previous papers [17–19]. The simulations consist of few steps. We start from the evaluation of the vibrational wave packet in the ground electronic state

$$\iota\frac{\partial}{\partial t}\phi(t) = \{H_0 - [\mathbf{d}\cdot\mathbf{E}_L(t)]\cos(\omega_L t + \varphi_L)\}\phi(t), \quad (8)$$

where H_0 is the nuclear Hamiltonian of the ground electronic state. Then, we compute the vibrational wave packet $\phi_c(t)$ in the potential of the core ionized state of the CO molecule and perform the Fourier transform $\phi_c(-\Omega)$

$$|\phi_c(t)\rangle = e^{iH_ct}\zeta|\phi(t)\rangle, \quad \zeta = \tfrac{1}{2}(\mathbf{e}_X \cdot \mathbf{D}_{c0})e^{i(\mathbf{k}_X - \mathbf{p})\cdot\mathbf{R}_A},$$

$$|\phi_c(-\Omega)\rangle = \int_{-\infty}^{\infty} dt\, e^{-i\Omega t} E_X(t)|\phi_c(t)\rangle, \tag{9}$$

where H_0 and H_c are the nuclear Hamiltonians of the ground and core ionized states, respectively; $\mathbf{D}_{c0}$ is the transition dipole moment of the core ionization process. The probability of x-ray absorption $P(\Omega)$ is given by the norm of the wave packet in the frequency domain [17,18]

$$P(\Omega) = \langle \phi_c(-\Omega)|\phi_c(-\Omega)\rangle. \tag{10}$$

Here, $\Omega = E_B - I_{1s}$ is the relative binding energy ($E_B = \omega_X - \varepsilon$), ε is the kinetic energy of the photoelectron, and I_{1s} is the adiabatic core ionization potential.

The initial wave function $|0\rangle$ and wave packets $\phi(t)$, $\phi_c(t)$, are calculated employing, respectively, time-independent and time-dependent techniques [20], implemented in the ESPEC program [21]. All the simulations are performed for fixed in-space molecules with the molecular axis being parallel to the polarization vector of the ir field $\mathbf{e}_L$.

IV. RESULTS

As it was already pointed out, the size of the ir-induced nuclear wave packet plays a crucial role in the enhancement of the recoil effect in XPS spectra. The proper choice of the intensity and the duration of the ir pulse allows one to get the vibrational wave packet with the desirable shape and size. Because of the Rabi oscillations, the size of the wave packet varies during interaction with the ir pulse. To measure the XPS spectrum using rather long x-ray pulse, it is desirable to keep the wave-packet size constant after the ir pulse leaves the system. Because of this, before going onto a detailed discussion of the manifestation of the recoil effect, we would like to give the outlines of the preparation of the vibrational wave.

A. Preparation of nuclear wave packet: Selective population of high vibrational levels

The wave packet created by the ir field is a coherent superposition of different vibrational states. In order to increase the size of the wave packet, higher vibrational levels ν should be populated. The vibrational levels up to $\nu = 16$ can be populated if the ir field has intensity $I_L = 2.3 \times 10^{14}$ W/cm^2 (see Figs. 4 and 5). Such an excitation increases the size of the wave packet almost four times in agreement with the estimation, $\sqrt{\nu + 1/2} \sim 4$ (see Fig. 1). Our simulations show that the ir pulse ($I_L = 2.3 \times 10^{14}$ W/cm^2, $\tau_L = 25$ or 50 fs) does not have time to dissociate molecule. The efficiency of ionization is even worse because of a strong deviation of ω_L from the frequency of electronic transition.

The dynamics of the populations ρ_ν are very sensitive to the relation between the Rabi frequency and the duration of the ir pulse, τ_L (Figs. 4 and 5). The permanent dipole moment depends almost linearly on the internuclear distance in the wave-packet region, $d(r) \approx d(r_e) + d'(r_e)(r - r_e)$. Because
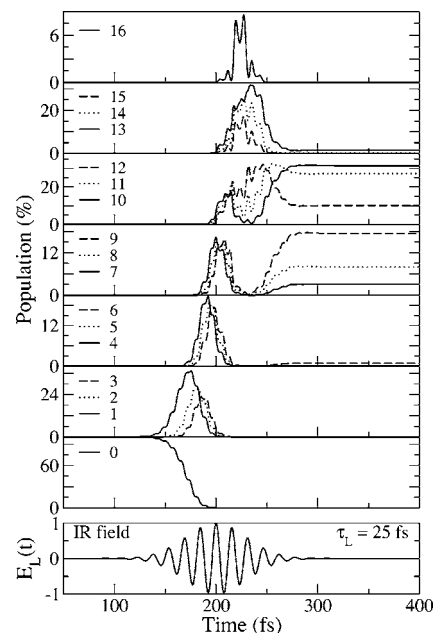
FIG. 5. Dynamics of populations ρ_ν of ground state vibrational levels $\nu = 0, \ldots, 16$ for $I_L = 2.3 \times 10^{14}$ W/cm^2, $t_L = 200$ fs and a short ir pulse $\tau = 25$ fs. The lowest panel displays the amplitude of the ir field normalized to the maximum.

of this, only the ladder transitions between adjacent vibrational levels are allowed, $\nu \to \nu \pm 1$. The corresponding Rabi frequency $G_{\nu+1,\nu} = \mathbf{E}_L \cdot \mathbf{d}_{\nu+1,\nu}$ strongly depends on ν. For instance,

$$G_{\nu+1,\nu} \approx G_{10}\sqrt{\nu + 1} \tag{11}$$

for isolated $\nu \leftrightarrow \nu + 1$ transition in harmonic potential. This means that the Rabi period $T_{\nu+1,\nu} = 2\pi/G_{\nu+1,\nu}$ decreases with an increase of ν, in agreement with the simulations, Figs. 4 and 5. Let us discuss two opposite cases: Long, $2\tau_L \gtrsim T_{10}$, and short, $2\tau_L < T_{10}$, ir pulse relative to the first Rabi period, $T_{10} \approx 130$ fs.

The evolution of the populations for rather long ir pulse, $2\tau_L = 100$ fs to $T_{10} \approx 130$ fs, is depicted in Fig. 4. In this case, the system performs only two Rabi oscillations. To enhance the recoil effect, we have to populate high vibrational states $\nu \gtrsim 7$. Figure 4 shows that these states are populated only near the peak position of the ir pulse. This means that the rather short x-ray pulse, $\tau_X < 100$ fs, with peak position near the ir pulse can be used in the case $2\tau_L \gtrsim T_{10}$.

From the point of view of the current experiment it is desirable to use longer x-ray pulses. To satisfy this requirement shorter ir pulses, $2\tau_L = 50$ fs $< T_{10} \approx 130$ fs, are preferable. The dynamics of the populations looks now qualitatively different (Fig. 5). The vibrational states $\nu \leq 6$ are almost completely depopulated after the ir pulse leaves the system, contrary to the vibrational states of our interest $\nu = 7-12$, which are now populated (see Fig. 5). These states are slowly depopulated because of the finite lifetime of the vibrational states. However, this lifetime is around 1 ns for
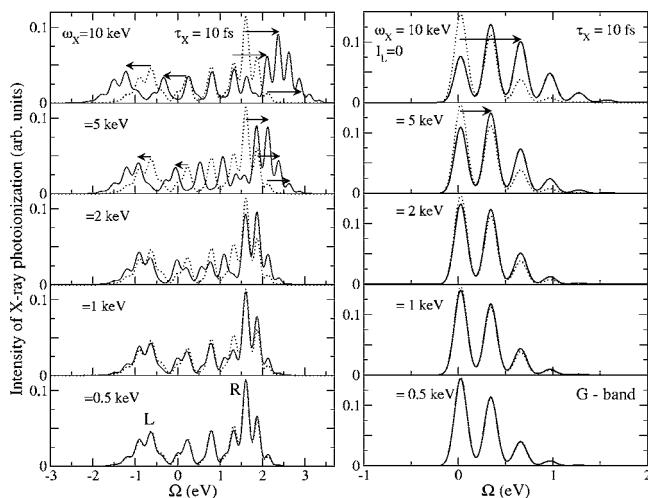
FIG. 6. C K XPS spectra of CO driven by an ir field. Long x-ray pulse, $\tau_X = 10$ fs. The horizontal arrows show red- and blueshifts of the L and R bands, respectively, with the increase of the x-ray photon energy. The dotted lines show the XPS spectrum without taking into account the recoil effect. Left and right panels display XPS spectra for $I_L = 2.3 \times 10^{14}$ W/cm^2 and $I_L = 0$, respectively.

FIG. 7. C K XPS spectra of CO driven by an ir field. Short x-ray pulse, $\tau_X = 3$ fs. The solid line shows the XPS spectrum without taking into account the recoil effect ($\theta = \pi/2$). The horizontal arrows show red- and blueshifts of the L and R bands, respectively, with the increase of the x-ray photon energy.

small molecules and is neglected here. Because the populations of the higher vibrational levels are large and almost constant for large times, one can use a long x-ray pulse. In the simulations presented below we will focus our attention only on this case of a rather short ir pulse (Fig. 5). We also use quite short x-ray pulses, $\tau_X = 10$ fs (except in Fig. 7). This duration is longer than the period of oscillations (≈ 4 fs) of the wave packet in the potential well, and therefore further increase of the τ_X does not change XPS spectra [18]. Our simulations show that the only role of the longer x-ray pulses is to increase the spectral resolution. Apparently, τ_X has to be shorter than the lifetime of vibrational excitation in the ground electronic state (~ 1ns to 1 ps). This means that rather long x-ray pulses from a synchrotron can be used for observation of the discussed effects.

The fast modulation of the Rabi oscillations (Figs. 4 and 5) deserves a special comment. The Rabi oscillations for low vibrational states are accompanied by weak modulations with the frequency $2\omega_L$ caused by the breakdown of the rotating wave approximation (RWA) [18,22]. Figures 4 and 5 show that these fast RWA-breaking modulations are enhanced drastically for $\nu = 15, 16$, where $G_{\nu+1,\nu} \sim \omega_L$.

B. C K XPS spectrum: Red- and blueshifts

Lets us start the analysis of the numerical simulations from the C K XPS spectra of the CO molecule without ir field (see the right panel in Fig. 6). In this case, the initial wave packet is nothing more than the wave function of the lowest vibrational level and the related XPS spectra (Fig. 6) correspond to the G transition in Fig. 1. The size of the wave packet is small and the factor $(1 - F_0/F_c)$ for the G band is positive and rather large (Fig. 3). Because of this, the role of the photoelectron momentum, or of the recoil effect, starts to be important for large photon energies [5] ($\gtrsim 5$ keV). We see
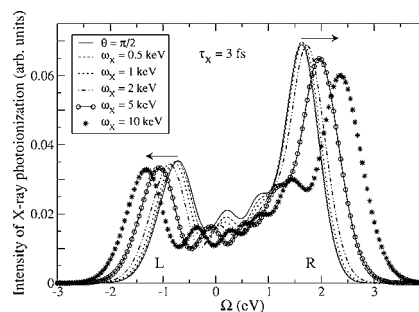
the blue spreading of the XPS band because of $(1 - F_0/F_c > 0)$. Let us pay attention to the shape of the XPS profile for 5 and 10 keV. The blue sideband of the XPS spectrum for 5 keV strongly reminds one of the profile of the XPS spectrum for $\omega_X \lesssim 2$ keV shifted on vibrational frequency $\Delta\omega = \omega_{10}$. The same effect is clearly seen for $\omega_X = 10$ keV. The difference here is a double shift of the band $\Delta\omega = 2\omega_{10}$, which is in nice agreement with Eq. (7) and Fig. 3 [see also the discussion of Eq. (12)].

The situation changes drastically when the CO molecule is shined by a strong ir field, which creates a wave packet with main contribution from the $\nu \approx 9-11$ vibrational states (see Fig. 6). The role of the photoelectron momentum starts to be important for smaller photon energies, in agreement with the estimation [5], $p \approx \pi/a_\nu \approx \pi\sqrt{\nu + 1/2}/a_0$. Because of the large size of these vibrational wave functions, the wave packet has now the left ($r_L = 1.846$ a.u.) and right ($r_R = 2.632$ a.u.) classical turning points. Figure 1 shows that the XPS transition has lower energy from the left turning point than from the right one. The factor $(1 - F_0/F_c)$ has the opposite sign for these turning points (Fig. 3), and the magnitude of this factor is considerably smaller in comparison to the case without an ir field. The opposite signs of $(1 - F_0/F_c)$ lead to the red- and blueshifts of the L and R band (see Figs. 1 and 6). One can see clearly that the L-band shift is smaller than the R-band shift. This is because the factor $|1 - F_0/F_c|$ has a smaller value for the R band (Fig. 3). The shorter x-ray pulse washes out the vibrational resolution and stresses this effect (Fig. 7). It is important to note that the individual vibrational resonances do not experience any shift. The recoil effect redistributes only the intensities of vibrational peaks. Although, such a redistribution of intensities looks like red- and blueshift of the center of gravities of the L and R sidebands (see panels $\omega_X = 5$ keV and $\omega_X = 10$ keV in Fig. 6).

For shifts (7) smaller than the vibrational frequency ($\Delta\omega < \omega_{10}$), one can see only the redistribution of the intensities of the resonances (Fig. 6). However, when

$$\Delta\omega = n\omega_{10}, \quad n = 1, 2, 3, \cdots \qquad (12)$$

a new band appears having almost the same profile as the band without taking into account the recoil effect. For larger
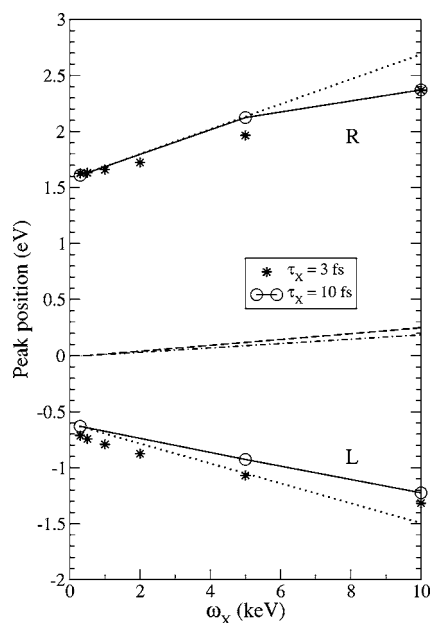
FIG. 8. Dispersion of the L- and R-bands of C K spectra of CO based on the wave-packet simulations. The dispersion given by the approximation (7) is shown by dotted lines. Dashed and dashed-dotted lines display internal recoil energy $E_{rec}^{(i)}$ for $\theta = 0$ deg and recoil energy of the molecular center of gravity, E_{rec} (5), respectively.

FIG. 9. O K XPS spectra of CO driven by an ir field. Long x-ray pulse, $\tau_X = 10$ fs. The horizontal arrows show red- and blueshifts of the R and L bands, respectively, with the increase of the x-ray photon energy. The dotted lines show the x-ray spectrum without taking into account the recoil effect. Left and right panels display XPS spectra for $I_L = 2.3 \times 10^{14}$ W/cm² and $I_L = 0$, respectively.

photon energy we note again only the redistribution of the intensity until $\Delta \omega = 2\omega_{10}$. Now one can observe clearly the formation of the new band (Fig. 6) shifted by $2\omega_{10}$, which again mimics the band without taking into account the recoil effect. In this sense, one can speak about periodical revival of the vibrational profile with a period equal to the vibrational frequency.

Figure 8 displays the dispersion laws for the L and R bands obtained from the wave-packet simulations depicted in Figs. 6 and 7. The dotted line in Fig. 8 is obtained using Eq. (7), with the gradients calculated in points $r_L = 1.846$ a.u. and $r_R = 2.632$ a.u., which correspond to the L and R bands (see Fig. 1). The agreement between the wave-packet simulations and Eq. (7) is rather good, but not perfect, because Eq. (7) is an approximation.

C. O K XPS spectrum

Contrary to the C K spectrum, oxygen core ionization from the left turning point results in a higher excitation energy in comparison to the right one (Fig. 1). One can expect that the role of the photoelectron momentum is larger in the XPS spectrum of oxygen because the potentials of the ground and core excited states are very similar (Fig. 1). This results in a very small difference of the gradients for the left turning point (Fig. 3). Indeed, the simulations show that the role of the photoelectron momentum in the O K spectra (Fig. 9) starts to be important for smaller photoelectron energies: $\omega_X - I_{1s} \approx 460$ eV than in the XPS spectra of carbon, $\omega_X - I_{1s} \approx 700$ eV (Fig. 6).

Unlike the carbon case, the factor $(1 - F_0/F_c)$ has the same sign for the L and R turning points and one can expect

that both L and R band will be redshifted for larger excitation energies. However, the simulations display a more sophisticated picture (Fig. 9). The R band moves to the red side in agreement with the sign of the factor $(1 - F_0/F_c)$ (Fig. 3). However, the L band is split into two parts that move in opposite directions when ω_X increases. The reason for the appearance of blueshift is the delocalization of the wave packet near the left turning point (Fig. 1). The delocalization of the wave packet is very important because the left turning point is very close to the point where the factor $(1 - F_0/F_c)$ changes the sign (Fig. 3). Because of this, the part of the wave packet near the left turning point has a positive sign of the factor $(1 - F_0/F_c)$, whereas the other part has the opposite sign of this factor. Therefore, part of the x-ray transitions occurs in the region where the shift $\Delta \omega$ (7) is negative, whereas the other transitions occur in the region with positive $\Delta \omega$. This explains the splitting of the L band in red- and blueshifted components. Because the L band is formed by transitions near to the point where $1 - F_0/F_c = 0$, the blue- and redshifts of this band are larger than the shift of the R band (Fig. 9). Such a splitting of the L band is absent for the R band because the factor $(1 - F_0/F_c)$ is negative in a broad region around the right turning point.

D. The same potentials of ground and core ionized states

The potentials of the core ionized oxygen and ground states are very similar, and because of this, the recoil effect in the O 1s spectra is enhanced when comparing them to the carbon spectra (see Figs. 6 and 9).

This motivates us to investigate the important model case where these potentials are exactly the same ground and core excited states. When the recoil effect is neglected, the XPS profile does not depend on the x-ray frequency and collapses with good accuracy to a single line because x-ray transitions without a change of the vibrational quantum number are al-
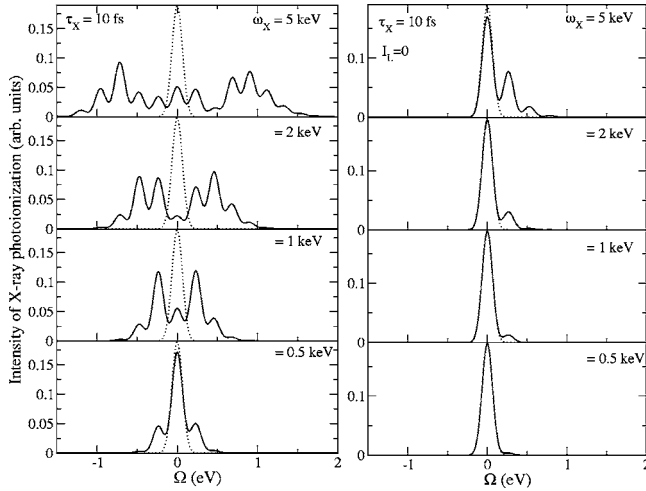
FIG. 10. C K XPS spectra of CO molecule in an ir field. Model case with the same potentials for the core ionized states. The dotted lines show the XPS spectra without taking into account the recoil effect. Left and right panels display XPS spectra for $I_L = 2.3 \times 10^{14}$ W/cm^2 and $I_L = 0$, respectively.

lowed (left panel in Fig. 10). The right panel of Fig. 10 shows that the role of the recoil effect is rather small in the case of the conventional XPS spectra without ir radiation ($I_L = 0$). The ir field enhances drastically the manifestation of the recoil effect (see Figs. 10 and 11). The reason for this that when the gradients F_0 and F_c are the same, Eq. (7) stops to be valid and, hence, this limiting case deserves special treatment. Let us write the FC amplitude in the momentum representation

$$\langle \nu | e^{-\imath \alpha \mathbf{q} \cdot \mathbf{r}} | \nu_0 \rangle = \int \varphi_\nu(k+q) \varphi_{\nu_0}(k) dk. \quad (13)$$

It is worth noting that the vibrational wave functions of the ground and core ionized states are now eigenfunctions of the
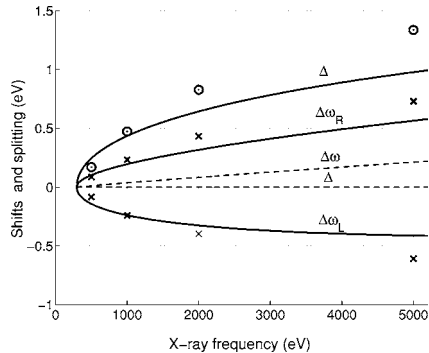
FIG. 11. Shifts ($\Delta\omega_{L,R}$) and splitting Δ (16) for the same potentials of the core ionized and ground state (C K XPS). The points correspond to the centers of gravity of the red and blue bands in Fig. 10. The splitting is calculated as the difference between these centers of gravity. The solid lines display the shifts and splitting (16) calculated for the Morse potential $U_0(r)$. The dashed lines display the shift $\Delta\omega = \Delta\omega_R = \Delta\omega_L$ and the splitting Δ for the case without an ir field.

same Hamiltonian. Taking into account that the Fourier transform $\varphi_\nu(k)$ of the vibrational wave function $\psi_\nu(x)$ of the harmonic oscillator is expressed again through Hermitian polynomials [23], we get the following important result for the generalized FC amplitude:

$$\int \psi_\nu(x) e^{-\imath \alpha \mathbf{q} \cdot \mathbf{r}} \psi_{\nu_0}(x) dx = \int \psi_\nu(x - \Delta r') \psi_{\nu_0}(x) dx. \quad (14)$$

This means that when the potential surfaces are the same, the only role of the momentum q is to shift effectively the core excited potential surface by

$$\Delta r' = \alpha q a_0^2 \cos \theta, \quad (15)$$

where $a_0 = 1/\sqrt{\mu\omega_0}$ is the size of the lowest vibrational wave function. Such a shift leads to the splitting of the XPS band, as illustrated in Fig. 2(b). This figure allows one to get a simple quasiclassical expression for the shift of the left and the right bands ($\Delta\omega_{L,R}$), as well as, for the spacing between these bands (Δ):

$$\Delta\omega_{L,R} = U_0(r_{L,R} + \Delta r') - U_0(r_{L,R}), \Delta = \Delta\omega_R - \Delta\omega_R. \quad (16)$$

In the simulations presented in Fig. 11 we used the following approximation: $r_L = r_e - a_\nu/2$ and $r_R = r_e + a_\nu/2$, where $a_\nu = a_0 \sqrt{\nu + 1/2}$ is the size of the νth vibrational wave function. When the ir field is absent, $r_L = r_R = r_e$, and because of this, $\Delta\omega_R = \Delta\omega_R = \Delta\omega$ and the splitting Δ is equal to zero. As one can see from Fig. 11 the ir field strongly increases the shifts and the splitting in agreement with the XPS spectra (Fig. 10).

V. SUMMARY

By changing the intensity and the duration of the ir pulse, one can shape the vibrational wave packet of desirable size. We demonstrate the strong enhancement of the recoil effect in XPS spectra of molecules driven by a strong ir field. The reason for this effect is twofold. The first is the ir-induced increase of the size of the vibrational wave packet. The second reason for the enhancement of the role of the photoelectron momentum is related to the gradients of the potentials of the ground and of the core excited states in the classical turning points of the wave packet. The role of the photoelectron momentum strongly increases when these gradients approach each other in the turning points. The different sides of the XPS band experience blue- and redshifts, depending on the sign of the gradient differences of the ground and core ionized states in the classical turning points. These shifts grow with the increase of the photon energy. When the shift grows beyond the vibrational energy, one can clearly see the revival of the vibrational sidebands. The dynamics of the XPS sidebands with the increase of the x-ray photon energy gives direct information about the shape of the interatomic potentials in the ground and core ionized states. It is worth emphasizing that the $1-100$ ps long x-ray pulses from a synchrotron can be used for observation of the discussed effect.

ACKNOWLEDGMENTS

APPENDIX: AIRY APPROXIMATION

Let us to expand the potentials of the ground, $U_0(r)$, and of the core excited state $U_c(r)$ near the point of vertical transition r_v

$$U_j(r) \approx U_j(r_v) + F_j x, \quad j = 0, c, \quad x = r - r_v, \quad \text{(A1)}$$

$$F_j = \left. \frac{dU_j}{dr} \right|_{r=r_v}.$$

Near these points, the energy normalized nuclear wave functions is given by the Airy function

$$\psi_j(x) = \sqrt{2\mu a_j} \, \text{Ai}\left(\mp \frac{x - \epsilon_j/F_j}{a_j} \right), \quad \epsilon_j = E_j - U_j(R_t), \quad \text{(A2)}$$

$$a_j = |2\mu F_j|^{-1/3},$$

where minus and plus correspond to the left ($F_j < 0$) and right ($F_j > 0$) turning points. The generalized FC amplitude reads ($F_c \neq F_0$)

$$\langle \psi_c(x) | e^{\iota q x} | \psi_0(x) \rangle = \frac{e^{\iota\theta}}{\gamma_{c0}} \text{Ai}\left(\eta \frac{1}{a} \left(\frac{\epsilon_c}{F_c} - \frac{\epsilon_0}{F_0} - \Delta R \right) \right). \quad \text{(A3)}$$

Here, $\eta = \sin(F_0 |-| F_c|)$ if $F_0 F_c > 0$ and $\eta = \sin(F_c)$ if $F_0 F_c < 0$, $\alpha = m_B/(m_A + m_B)$, while θ is the angle between $\mathbf{q}$ and $\mathbf{R}$.

$$a = \sqrt{a_0 a_c} \left| \frac{F_c - F_0}{F} \right|^{1/3}, \quad \gamma_{c0} = aF = \left| \frac{(F_c - F_0)F}{2\mu} \right|^{1/3}, \quad \text{(A4)}$$

$$F = \sqrt{|F_0 F_c|}.$$

The FC amplitude (A3) takes maximum when

$$\frac{\epsilon_c}{F_c} - \frac{\epsilon_0}{F_0} = \Delta R. \quad \text{(A5)}$$

The ground-state wave packet $\phi(t)$ has maximum near the turning point, where $\epsilon_0 = 0$. When the recoil effect is neglected, Eq. (A5) means that the transition is vertical and $\epsilon_c = 0$. The recoil effect makes the x-ray transition nonvertical, $\Delta R \neq 0$, and this results in the shift of the XPS sideband by $\Delta\omega = \epsilon_c = F_c \Delta R$ [see Eq. (7)].

[1] S. Svanberg, *Atomic and Molecular Spectroscopy: Basic Aspects and Practical Applications* (Springer, New York, 2001).

[2] K. J. Randall, A. L. D. Kilcoyne, H. M. Köppe, J. Feldhaus, A. M. Bradshaw, J.-E. Rubensson, W. Eberhardt, Z. Xu, P. D. Johnson, and Y. Ma, Phys. Rev. Lett. **71**, 1156 (1993).

[3] A. Föhlisch, J. Hasselström, O. Karis, P. Väterlein, N. Mårtensson, A. Nilsson, C. Heske, M. Stichler, C. Keller, W. Wurth, and D. Menzel, Chem. Phys. Lett. **315**, 194 (1999).

[4] W. Domcke and L. S. Cederbaum, Chem. Phys. Lett. **13**, 161 (1978).

[5] F. Gel'mukhanov, P. Sałek, and H. Ågren, Phys. Rev. A **64**, 012504 (2001).

[6] M. Drescher, Z. phys. Chem. **218**, 1147 (2004).

[7] G. G. Paulus, F. Grasbon, H. Walther, P. Villoresi, M. Nisoli, S. Stagira, E. Priory, and S. De Silvestri, Nature (London) **414**, 182 (2001).

[8] T. Beddar, W. Sibbett, D. T. Reid, J. Garduno-Mejia, N. Jamasbi, and M. Mohebi, Opt. Lett. **24**, 163 (1999).

[9] J. A. Gruetzmacher and N. F. Scherer, Rev. Sci. Instrum. **73**, 2227 (2002).

[10] H.-S. Tan and W. S. Warren, Opt. Express **11**, 1021 (2003).

[11] K. P. Huber and G. Herzberg, *Molecular Spectra and Molecular Structure IV*, (Van Nostrand Reinhold, New York, 1979).

[12] M. Tronc, G. C. King, and F. Read, J. Phys. B **12**, 137 (1979).

[13] U. Gelius, S. Svensson, H. Siegbahn, E. Basilier, Å. Faxälv, and K. Siegbahn, Chem. Phys. Lett. **28**, 1 (1974).

[14] T. Helgaker, H. J. Aa. Jensen, P. Jørgensen, J. Olsen, K. Ruud, H. Ågren, A. A. Auer, K. L. Bak, V. Bakken, O. Christiansen, S. Coriani, P. Dahle, E. K. Dalskov, T. Enevoldsen, B. Fernandez, C. Hättig, K. Hald, A. Halkier, H. Heiberg, H. Hettema, D. Jonsson, S. Kirpekar, R. Kobayashi, H. Koch, K. V. Mikkelsen, P. Norman, M. J. Packer, T. B. Pedersen, T. A. Ruden, A. Sanchez, T. Saue, S. P. A. Sauer, B. Schimmelpfenning, K. O. Sylvester-Hvid, P. R. Taylor, O. Vahtras, *Dalton, A Molecular Electronic Structure Program*, Release 1.2, 2001. See http://www.kjemi.uio.no/software/dalton/dalton.html

[15] T. H. DunningJr., J. Chem. Phys. **90**, 1007 (1989).

[16] R. A. Kendall, T. H. Dunning Jr., and R. J. Harrison, J. Chem. Phys. **96**, 6796 (1992).

[17] V. C. Felicíssimo, F. F. Guimarães, F. Gel'mukhanov, A. Cesar, and H. Ågren, J. Chem. Phys. **122**, 094319 (2005).

[18] F. F. Guimarães, V. Kimberg, V. C. Felicíssimo, F. Gel'mukhanov, A. Cesar, and H. Ågren, Phys. Rev. A **72**, 012714 (2005).

[19] F. F. Guimarães, F. Gel'mukhanov, A. Cesar, and H. Ågren, Chem. Phys. Lett. **405**, 398 (2005).

[20] C. Leforestier, R. H. Bisseling, C. Cerjan, M. D. Feit, R. Friesner, A. Guldberg, A. Hammerich, G. Jolicard, V. Karrlein, H. D. Meyer, N. Lipkin, O. Roncero, R. Kosloff, J. Comput. Phys. **94**, 59 (1991).

[21] F. F. Guimarães, V. C. Felicíssimo, V. Kimberg, A. Cesar, and

F. Gel'mukhanov, eSPec wave packet propagation program, Universidade Federal de Minas Gerais, Brazil and Royal Institute of Technology, Sweden (2004), See http://www.theochem.kth.se/people/freddy/

[22] M. S. Shahriar, P. Pradhan, and J. Morzinski, Phys. Rev. A **69**, 032308 (2004).

[23] L. D. Landau and E. M. Lifshitz, *Quantum Mechanics* (Pergamon Press, London, 1962).